Title
Single gate p-n junctions in graphene-ferroelectric devices

Journal
Applied Physics Letters, 108(20)

ISSN
0003-6951

Authors
Hinnefeld, J Henry
Xu, Ruijuan
Rogers, Steven
et al.

Publication Date
2016-05-16

DOI
10.1063/1.4950975

Peer reviewed

Single gate p-n junctions in graphene-ferroelectric devices

J. Henry Hinnefeld, Ruijuan Xu, Steven Rogers, Shishir Pandya, Moonsub Shim, Lane W. Martin, and Nadya Mason

Citation: Applied Physics Letters **108**, 203109 (2016); doi: 10.1063/1.4950975
View online: http://dx.doi.org/10.1063/1.4950975
View Table of Contents: http://scitation.aip.org/content/aip/journal/apl/108/20?ver=pdfcov
Published by the AIP Publishing

Single gate p-n junctions in graphene-ferroelectric devices

J. Henry Hinnefeld,[1] Ruijuan Xu,[2,3] Steven Rogers,[4] Shishir Pandya,[2,3] Moonsub Shim,[4] Lane W. Martin,[2,3] and Nadya Mason[1,a)]
[1]*Department of Physics, University of Illinois at Urbana-Champaign, Urbana, Illinois 61801, USA*
[2]*Department of Materials Science and Engineering, University of California, Berkeley, California 94720, USA*
[3]*Materials Science Division, Lawrence Berkeley National Laboratory, Berkeley, California 94720, USA*
[4]*Department of Materials Science and Engineering, University of Illinois at Urbana-Champaign, Urbana, Illinois 61801, USA*

(Received 29 January 2016; accepted 7 May 2016; published online 19 May 2016)

Graphene's linear dispersion relation and the attendant implications for bipolar electronics applications have motivated a range of experimental efforts aimed at producing p-n junctions in graphene. Here we report electrical transport measurements of graphene p-n junctions formed via simple modifications to a $PbZr_{0.2}Ti_{0.8}O_3$ substrate, combined with a self-assembled layer of ambient environmental dopants. We show that the substrate configuration controls the local doping region, and that the p-n junction behavior can be controlled with a single gate. Finally, we show that the ferroelectric substrate induces a hysteresis in the environmental doping which can be utilized to activate and deactivate the doping, yielding an "on-demand" p-n junction in graphene controlled by a single, universal backgate. *Published by AIP Publishing.*
[http://dx.doi.org/10.1063/1.4950975]

Graphene is a subject of intense research interest due to the enormous potential of its electronic and mechanical properties.[1] In particular, p-n junctions in graphene have great potential for both fundamental research and commercial applications, and have been utilized to study the quantum Hall effect[2–4] and Klein tunneling[5,6] as well as to fabricate flexible transistors.[7] Previous work on p-n junctions in graphene employed multiple electrostatic gates,[2–6,8–11] charge transfer from the controlled deposition of chemical adsorbates,[12–18] high current-induced charging of trap states in the substrate,[19] or periodically poled ferroelectric substrates.[20]

In this letter, we report the fabrication of p-n junctions in graphene deposited on a uniformly poled ferroelectric substrate. The local doping in our devices is accomplished by combining simple modifications to a lead zirconium titanate ($PbZr_{0.2}Ti_{0.8}O_3$) substrate—the evaporation of thin SiO_2 films in some regions—with a self-assembled layer of environmental dopants. We find that the $PbZr_{0.2}Ti_{0.8}O_3$ substrate modulates the doping effect of the adsorbed dopants: devices are exposed to ambient conditions after fabrication whereupon experimental observations confirm both the presence of adsorbed dopants (likely primarily H_2O) and their enhanced doping effect on the $PbZr_{0.2}Ti_{0.8}O_3$ relative to the SiO_2. Furthermore, we demonstrate that the $PbZr_{0.2}Ti_{0.8}O_3$ substrate induces a hysteresis in the environmental doping which can be used to activate and deactivate the doping via the application of large gate voltages. We employ this effect to create p-n junctions which can be reversibly transitioned between p-n junction and uniformly conducting configurations.

Devices consist of graphene micro-ribbons deposited on substrates which are partially covered by a thin layer of evaporated SiO_2, and contacted in a four-point geometry, as illustrated in Figures 1(a)–1(c). An SEM micrograph of a typical device is shown in the inset of Figure 1(d). The devices are fabricated using standard lithography and deposition techniques on thin-film ferroelectric substrates. For the ferroelectric substrates, 120 nm thick (001)-oriented lead zirconium titanate ($PbZr_{0.2}Ti_{0.8}O_3$) films are prepared by pulsed-laser deposition (PLD) on a strontium titanate ($SrTiO_3$) substrate coated with 20 nm of strontium ruthenate ($SrRuO_3$), following established procedures.[21,22] For each substrate, an 80 nm-thick layer of SiO_2 is evaporated in small rectangular regions, with region widths ranging from 0.5 μm to 3 μm, as illustrated in Figs. 1(a)–1(c). CVD graphene is then transferred using standard wet transfer techniques,[23] and patterned into ribbons spanning the deposited SiO_2 using photolithography and reactive ion etching. The graphene channel is 6 μm by 4 μm measured from the inner contacts. Control devices which span regions with no evaporated SiO_2 are also fabricated. Finally, Cr/Au (3 nm/20 nm) leads are

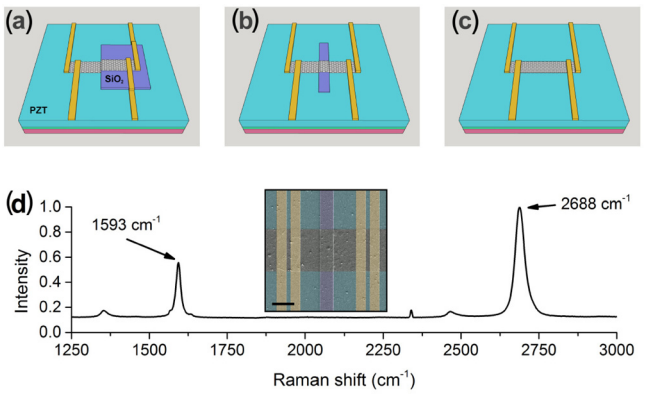

FIG. 1. (a)–(c) Schematic illustration of the device geometry. The graphene (grey) spans the regions of evaporated SiO_2 (purple) on the bare substrate (teal) and is contacted by Cr/Au electrodes (yellow). The universal backgate is shown in red. (d) Raman spectra of graphene from a device fabricated on a thermal SiO_2 substrate. Inset: a false-color SEM micrograph of a representative device. The scale bar is 2 μm.

a)nadya@illinois.edu

deposited in a four-point measurement configuration. Raman spectroscopy is used to confirm the monolayer character and high quality of the graphene after fabrication; representative spectra are shown in Figure 1(d).

Transport measurements in air are performed using two Keithley 2400 SourceMeters. Measurements in vacuum are performed using an Agilent 4156 C Semiconductor Parameter Analyzer. In both cases, source-drain current is measured with a constant source-drain bias of 5 mV, while the voltage applied to the backgate is swept. Gate leakage distorts transport results for gate voltages more positive than 1.5 V or more negative than −1 V, so gate voltages are limited to this range. Gate voltage sweep rates range from 10 mV/s to 100 mV/s; the data presented here are from sweeps at 100 mV/s. Slower sweep rates yield qualitatively similar results.

Figure 2(a) shows room temperature I_{sd} vs V_{gate} curves for devices having different widths of evaporated SiO_2 on a $PbZr_{0.2}Ti_{0.8}O_3$ substrate. For the data shown here, the fraction of the graphene channel screened by evaporated SiO_2 ranges from 0% to 50% (corresponding to SiO_2 widths of 0 to 3 μm). Two features of the data are immediately apparent: first, for devices which span an evaporated SiO_2 region, the characteristic conductance minimum typically observed in graphene at the Dirac point is split into two distinct minima, one at the original Dirac point location and a second shifted to the right. This is apparent in the top and bottom curves of the figure: the bottom curve, corresponding to a device with 0% screening, displays a single minimum, while the top curve, corresponding to a device with 50% screening, displays two pronounced minima. Second, the width of the evaporated SiO_2 region determines which of the two minima has a smaller absolute value. As the screening fraction is increased, "weight" is transferred from the minimum at the original Dirac point location to the secondary minimum, and

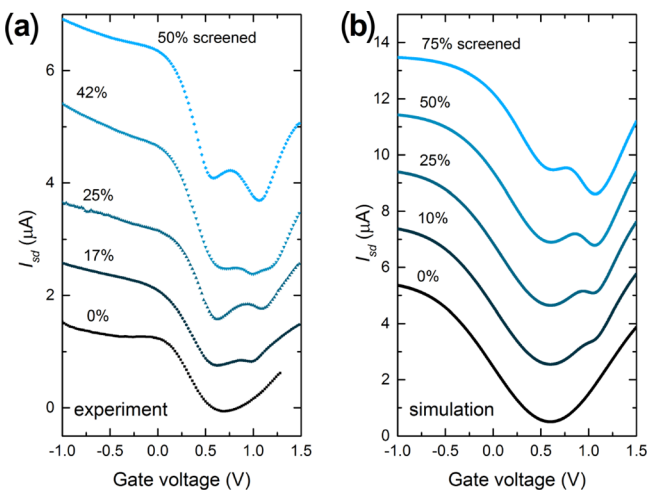

FIG. 2. (a) I_{sd} vs V_{gate} curves (manually offset for clarity) for devices having different widths of evaporated SiO_2 on a $PbZr_{0.2}Ti_{0.8}O_3$ substrate. The devices having evaporated SiO_2 show split Dirac points, and the relative dominance of the left and right Dirac points can be tuned by varying the evaporated SiO_2 width. (b) Simulations of transport across a graphene device having two different locally doped regions, as a function of applied gate voltage. The simulations show both Dirac point splitting and variations in left vs. right Dirac point dominance as a function of screening region width, consistent with the experimental data.

the depths of the two minima vary accordingly. We attribute both of these effects to the presence of two different doping regions in the graphene, defined by the $PbZr_{0.2}Ti_{0.8}O_3$ substrate and the evaporated SiO_2.

The data can be understood by considering that as the gate voltage is swept from negative to positive, the Fermi level passes through the charge-neutrality point (CNP) of each graphene region separately. Taking the conductance to be linear with carrier density[24] $\sigma \propto k_F\langle\tau\rangle \propto n$ and the carrier density to be linear with the thermally smeared energy difference between the Fermi level and the CNP,[25] we model the conductance in the vicinity of the CNP as: $\rho^{-1} \propto n \propto 1 - e^{-(V_{gate}-\mu-\delta)^2/2c^2} + \epsilon$ where the constant μ accounts for the extrinsic doping introduced by the fabrication process, $\delta \in \{0, 1\}$ describes the substrate-dependent doping, and ϵ accounts for the non-vanishing carrier density at the CNP. Assuming diffusive transport in the graphene, the relative weight of each separately doped region, and therefore the relative magnitude of the measured conductance minima, is determined by the fraction of the graphene channel which is screened:

$$I_{sd} \propto [\rho_{scr.} \times (\text{pct.}_{\text{scr.}}) + \rho_{\text{non-scr.}} \times (\text{pct.}_{\text{non-scr.}})]^{-1}.$$

This is simulated in Figure 2(b) which shows I_{sd} vs V_{gate} curves for screening fractions ranging from 0% to 75% and is in excellent agreement with our experimental data. We note that the simulations agree with our data for $\mu > 0$ and $\delta \geq 0$, which is consistent with the extrinsic p-doping typically observed in graphene devices fabricated on $PbZr_{0.2}Ti_{0.8}O_3$.[26]

The substrate-selectivity of the doping in our devices suggests that the ambient dopants are polar H_2O molecules. Polar surface adsorbates have been shown to dramatically affect the electronic properties of complex oxide systems[27] as well as graphene.[13,28,29] The H_2O doping is substrate-selective because of the unique ferroelectric nature of the $PbZr_{0.2}Ti_{0.8}O_3$ substrate. Previous work[30,31] has established the importance of the orbital structure of the adsorbate in determining the most energetically favorable orientation. For standard graphene devices on SiO_2 substrates, the structure of H_2O favors a uniform polarization throughout the range of applicable gate voltages. For graphene on ferroelectric substrates however, previous work[29] indicates that electrostatic effects of the remnant polarization and substrate lattice geometry can modulate the stability of the H_2O polarization. In the devices described here, it is likely that the interaction between the remnant polarization of the $PbZr_{0.2}Ti_{0.8}O_3$ substrate and the H_2O molecules sufficiently alters the energetics of different H_2O orientations as to destroy the stability of the H_2O polarization, and thus create less-polarized regions. This hypothesis is in agreement with data collected from similar devices fabricated on non-ferroelectric substrates; such devices show none of the characteristic Dirac point splitting associated with p-n junctions.

The gate-voltage dependence of the H_2O polarization configurations on $PbZr_{0.2}Ti_{0.8}O_3$ vs SiO_2 leads to hysteresis in the devices. This can be seen in Figure 3(a), which shows I_{sd} vs V_{gate} curves for forward and reverse gate sweeps performed on the same devices as measured in Fig. 2(a). A

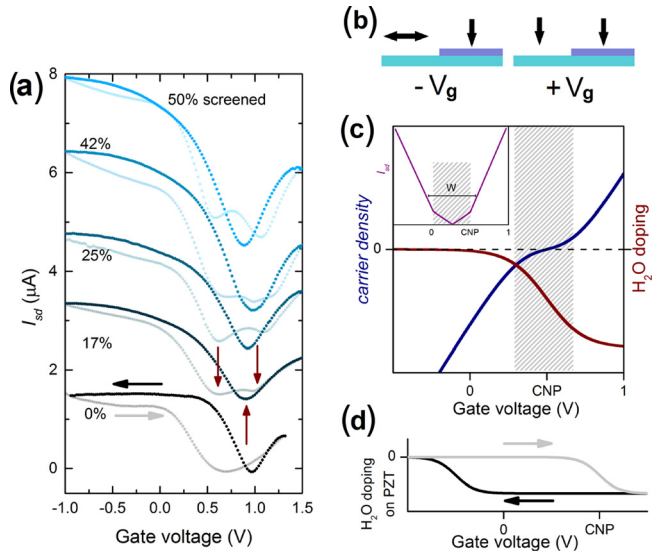

FIG. 3. (a) I_{sd} vs V_{gate} curves (manually offset for clarity) for forward (light) and reverse (dark) gate voltage sweeps. Representative minima locations are indicated by the vertical arrows. (b) H_2O polarization by device region, as prepared by positive and negative gate voltages. For negative gate voltages, H_2O on the $PbZr_{0.2}Ti_{0.8}O_3$ region is unpolarized, and H_2O on the SiO_2 region is polarized. For positive gate voltages, both regions have a net polarization. (c) Simulated carrier density vs. applied gate voltage. The onset of H_2O polarization is indicated by grey shading. Inset: simulated conductance vs. applied gate voltage. (d) A schematic illustration of the H_2O doping hysteresis with applied gate voltage; arrows indicate the direction of the gate voltage sweep.

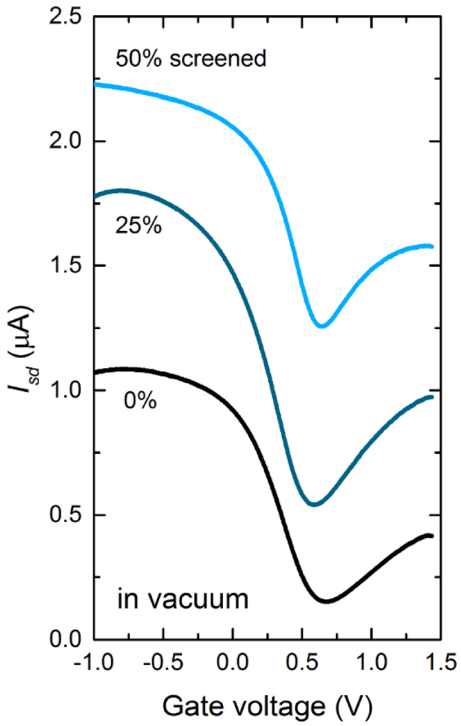

FIG. 4. Offset I_{sd} vs V_{gate} curves for devices measured in vacuum. The Dirac point splitting effect disappears in vacuum, but can be recovered by leaving the device in ambient conditions overnight.

pronounced hysteresis between forward and reverse gate sweeps is apparent. As in Fig. 2(a), devices spanning a region of evaporated SiO_2 display two distinct minima during forward sweeps, while a control device having no SiO_2 displays a single minimum. However, all devices display a single minimum during reverse gate sweeps. We note that the gate voltages applied here remain below the coercive voltage of the $PbZr_{0.2}Ti_{0.8}O_3$ film; therefore, ferroelectric switching is not a possible cause of the observed hysteresis. Ferroelectric switching has been shown to produce similar behavior;[32] however, in this work gate voltages above the coercive voltage of the film are experimentally inaccessible due to large gate leakage in our devices.

In order to understand how the hysteresis is related to the different H_2O polarization configurations on the $PbZr_{0.2}Ti_{0.8}O_3$ as compared to the evaporated SiO_2, it is instructive to consider the gate voltages at which the various minima appear. For example, for the 17% screened curve in Fig. 3(a) the red arrows point out two minima on the forward sweep (at 0.6 V and 1.1 V) and one minimum on the reverse sweep (at 0.9 V). These can be compared to the position of the Dirac point in vacuum at 0.6 V (see Fig. 4). The minimum on the forward sweep at 0.6 V occurs at the same gate voltage as the vacuum Dirac point, implying that it corresponds to a region of the graphene without a net polarization in the adsorbed H_2O. The remaining minima occur at voltages larger than the Dirac point (0.9 V and 1.1 V) and thus correspond to regions of the graphene on which the adsorbed H_2O is polarized and produces p-doping. Polarized H_2O typically produces p-doping in graphene, though the precise mechanism is the subject of continuing research.[30,33–36] We identify the forward-sweep minimum at 0.6 V as corresponding to graphene on the non-screened $PbZr_{0.2}Ti_{0.8}O_3$ region. This is supported by the fact that all devices demonstrate a minimum at 0.6 V, independent of different SiO_2 screening fractions. In contrast, the minimum indicated by the rightmost arrow (e.g., at 1.1 V for the 17% screened device) corresponds to graphene on the evaporated SiO_2 region, as evidenced by its evolution with increasing SiO_2 screening fraction.

We conclude that the application of a negative gate voltage destroys the net polarization of adsorbed H_2O on $PbZr_{0.2}Ti_{0.8}O_3$, but preserves a net polarization on the SiO_2-screened regions. This creates different local doping levels and thus a p-n junction. A positive gate voltage establishes a net polarization in both regions, and thus a uniform channel with no p-n junction, as depicted in Figure 3(b). This interpretation is further corroborated by the different widths of the forward and reverse minima for the control (0% screened) device, as evident in Fig. 3(a). This difference can be explained by considering that conductance is linear with carrier density,[24] so the width of the conductance minimum at the Dirac point is determined by the slope of the carrier density vs. gate voltage curve. Typically, the slope is constant, determined by the gate capacitance. However, for our devices the onset of H_2O dipole doping introduces a nonlinearity in the regime where the adsorbed H_2O transitions from unpolarized to polarized; this is shown schematically in Fig. 3(c). The polarized H_2O in our devices p-dopes the graphene, so the onset of its doping contribution temporarily reduces the slope of the carrier density vs. gate voltage curve, broadening the conductance minimum. During reverse sweeps, the transition from polarized to unpolarized H_2O occurs far from the CNP, so the width of the conductance minimum is unaffected. The hysteresis in H_2O polarization

is illustrated schematically in Figure 3(d). Experimentally, the polarization hysteresis displays a dependence on both the magnitude of the applied gate voltage and the duration of its application, which prevents an exact determination of the gate voltages required to establish or destroy the H_2O polarization.

The hysteresis of the H_2O polarization on $PbZr_{0.2}Ti_{0.8}O_3$ substrates adds an "on/off" switching element to the p-n behavior. Specifically, we can selectively transition the device into and out of the p-n junction configuration through the application of large positive and negative gate voltages. The initial application of a large positive gate voltage establishes a uniform polarization across the device, yielding a unipolar conducting channel, while a large negative gate voltage destabilizes the polarization on regions supported by $PbZr_{0.2}Ti_{0.8}O_3$. In the latter case, the different H_2O polarizations create separate locally doped regions, and thus a p-n junction. This "on/off" switching is different than the standard gate induced switching observed in p-n junctions, for example, from p-n to p^+-p. By comparison, in our devices the same applied gate voltage can generate either a p-n junction or a uniformly doped channel, depending on the H_2O polarization condition.

The ferroelectric nature of the $PbZr_{0.2}Ti_{0.8}O_3$ substrate might suggest that the residual electric field from the substrate polarization dopes the regions of graphene in direct contact with the substrate,[26,37] but has less effect in the graphene regions screened by evaporated SiO_2. Similarly, graphene-ferroelectric interfaces are known to have complex interfacial charge trap dynamics which can generate similar transport signatures.[32] However, both explanations are precluded by several further experimental observations. First, the Dirac point splitting effect disappears when the devices are measured in vacuum. Figure 4 shows I_{sd} vs V_{gate} curves for the same devices measured at 5×10^{-6} Torr, but otherwise under conditions identical to those of Figure 2(a). All devices show a single minimum, independent of evaporated SiO_2 width or gate sweep rate. Second, leaving the devices in ambient conditions overnight recovers the splitting effect. The observed behavior is consistent with an ambient dopant mechanism, i.e., the substrate-selective formation of a self-assembled layer of dopant molecules. In vacuum, dopant molecules desorb from the surface, leaving all regions of the graphene identically doped. Leaving the device in ambient conditions allows the dopant layer to reassemble, thereby re-establishing the separately doped regions.

The absence of Dirac point splitting in vacuum measurements also eliminates differences in gate capacitance as a dominant source of the splitting effect. The screened and non-screened regions of the device have different gate thicknesses and dielectric constants, which might suggest that the application of the same gate voltage would generate different doping levels in each region, and hence the transport behavior we observe. However, any capacitive differences between the regions are static, depending only on the geometry of the device, while the Dirac point splitting effect is dynamic, disappearing in vacuum. Capacitance-based explanations are further ruled out by the nearly identical Dirac point locations observed in all devices under vacuum. In particular, the similarity of data under vacuum from the control device (having no evaporated SiO_2), and from the devices which do span an evaporated SiO_2 region confirms that gate capacitance differences between the two regions are not the primary cause of the Dirac point splitting effect.

In summary, we have fabricated a controllable p-n junction in graphene on a ferroelectric substrate. We employ simple substrate modifications to define local doping regions, where the doping is accomplished through the substrate-selective formation of a self-assembled layer of ambient doping molecules. Alternative explanations for the local doping effect are ruled out, and the dynamics of the ambient doping suggest that it is due to polar H_2O molecules. Finally, the $PbZr_{0.2}Ti_{0.8}O_3$ substrate creates a hysteresis in the ambient doping effect which can be used to controllably bias the device into and out of a p-n junction configuration, using a single, universal backgate.

J.H.H., R.X., S.R., and M.S. acknowledge support from the National Science Foundation and the Nanoelectronics Research Initiative under NSF-NEB Grant No. DMR-1124696. S.P. acknowledges support from the Army Research Office under Grant No. W911NF-14-1-0104. N.M. and L.W.M. acknowledge support from the National Science Foundation under Grant No. ENG-1434147. This work was carried out in part in the Frederick Seitz Materials Research Laboratory Central Facilities at the University of Illinois.

[1]A. K. Geim and K. S. Novoselov, Nat. Mater. **6**, 183 (2007).
[2]J. R. Williams, L. Dicarlo, and C. M. Marcus, Science **317**, 638 (2007).
[3]B. Özyilmaz, P. Jarillo-Herrero, D. Efetov, D. Abanin, L. Levitov, and P. Kim, Phys. Rev. Lett. **99**, 166804 (2007).
[4]J. Velasco, G. Liu, L. Jing, P. Kratz, H. Zhang, W. Bao, M. Bockrath, and C. N. Lau, Phys. Rev. B **81**, 121407 (2010); e-print arXiv:0912.3179.
[5]N. Stander, B. Huard, and D. Goldhaber-Gordon, Phys. Rev. Lett. **102**, 026807 (2009).
[6]A. F. Young and P. Kim, Nat. Phys. **5**, 222 (2009).
[7]B. J. Kim, H. Jang, S. K. Lee, B. H. Hong, J. H. Ahn, and J. H. Cho, Nano Lett. **10**, 3464 (2010).
[8]I. Meric, M. Y. Han, A. F. Young, B. Ozyilmaz, P. Kim, and K. L. Shepard, Nat. Nanotechnol. **3**, 654 (2008).
[9]B. Huard, J. Sulpizio, N. Stander, K. Todd, B. Yang, and D. Goldhaber-Gordon, Phys. Rev. Lett. **98**, 236803 (2007).
[10]G. Liu, J. Velasco, W. Bao, and C. N. Lau, Appl. Phys. Lett. **92**, 203103 (2008).
[11]J. Velasco, G. Liu, W. Bao, and C. N. Lau, New J. Phys. **11**, 095008 (2009).
[12]D. B. Farmer, Y.-M. Lin, A. Afzali-Ardakani, and P. Avouris, Appl. Phys. Lett. **94**, 213106 (2009).
[13]T. Lohmann, K. von Klitzing, and J. H. Smet, Nano Lett. **9**, 1973 (2009).
[14]K. Brenner and R. Murali, Appl. Phys. Lett. **96**, 063104 (2010).
[15]H. C. Cheng, R. J. Shiue, C. C. Tsai, W. H. Wang, and Y. T. Chen, ACS Nano **5**, 2051 (2011).
[16]H. Sojoudi, J. Baltazar, L. M. Tolbert, C. L. Henderson, and S. Graham, ACS Appl. Mater. Interfaces **4**, 4781 (2012).
[17]B. H. Seo, J. Youn, and M. Shim, ACS Nano **8**, 8831 (2014).
[18]M. Park, Y. J. Yun, M. Lee, D. H. Jeong, Y. Jun, Y. W. Park, and B. H. Kim, AIP Adv. **5**, 017120 (2015).
[19]H.-Y. Chiu, V. Perebeinos, Y.-M. Lin, and P. Avouris, Nano Lett. **10**, 4634 (2010).
[20]C. Baeumer, D. Saldana-Greco, J. M. P. Martirez, A. M. Rappe, M. Shim, and L. W. Martin, Nat. Commun. **6**, 6136 (2015).
[21]R. Xu, S. Liu, I. Grinberg, J. Karthik, A. R. Damodaran, A. M. Rappe, and L. W. Martin, Nat. Mater. **14**, 79 (2014).
[22]J. Karthik, A. R. Damodaran, and L. W. Martin, Phys. Rev. Lett. **108**, 167601 (2012).
[23]X. Li, W. Cai, J. An, S. Kim, J. Nah, D. Yang, R. Piner, A. Velamakanni, I. Jung, E. Tutuc, S. K. Banerjee, L. Colombo, and R. S. Ruoff, Science **324**, 1312 (2009).

[24]E. Hwang, S. Adam, and S. Sarma, Phys. Rev. Lett. **98**, 186806 (2007).
[25]A. H. Castro Neto, N. M. R. Peres, K. S. Novoselov, and A. K. Geim, Rev. Mod. Phys. **81**, 109 (2009).
[26]C. Baeumer, S. P. Rogers, R. Xu, L. W. Martin, and M. Shim, Nano Lett. **13**, 1693 (2013).
[27]Y. Xie, Y. Hikita, C. Bell, and H. Y. Hwang, Nat. Commun. **2**, 494 (2011); e-print arXiv:1105.3891.
[28]F. Schedin, A. K. Geim, S. V. Morozov, E. W. Hill, P. Blake, M. I. Katsnelson, and K. S. Novoselov, Nat. Mater. **6**, 652 (2007); e-print arXiv:0610809 [cond-mat].
[29]H. Lu, A. Lipatov, S. Ryu, D. J. Kim, H. Lee, M. Y. Zhuravlev, C. B. Eom, E. Y. Tsymbal, A. Sinitskii, and A. Gruverman, Nat. Commun. **5**, 5518 (2014).
[30]O. Leenaerts, B. Partoens, and F. M. Peeters, Phys. Rev. B **77**, 125416 (2008).
[31]O. Leenaerts, B. Partoens, and F. M. Peeters, Phys. Rev. B **79**, 235440 (2009).
[32]N. Park, H. Kang, J. Park, Y. Lee, Y. Yun, J.-H. Lee, S.-G. Lee, Y. H. Lee, and D. Suh, ACS Nano **9**, 10729 (2015).
[33]J. Moser, A. Verdaguer, D. Jinez, A. Barreiro, and A. Bachtold, Appl. Phys. Lett. **92**, 123507 (2008); e-print arXiv:0803.2032.
[34]H. Wang, Y. Wu, C. Cong, J. Shang, and T. Yu, ACS Nano **4**, 7221 (2010); e-print arXiv:1011.0579.
[35]T. O. Wehling, A. I. Lichtenstein, and M. I. Katsnelson, Appl. Phys. Lett. **93**, 202110 (2008); e-print arXiv:0809.2894.
[36]J. Sabio, C. Seoánez, S. Fratini, F. Guinea, A. H. C. Neto, and F. Sols, Phys. Rev. B **77**, 195409 (2008); e-print arXiv:0712.2232.
[37]Y. Zheng, G.-X. Ni, C.-T. Toh, C.-Y. Tan, K. Yao, and B. Özyilmaz, Phys. Rev. Lett. **105**, 166602 (2010).